Rational Function Approximation of Transformer Branch Impedance Matrix For Frequency-Dependent White-Box Modeling

Bjørn Gustavsen, *Fellow, IEEE*

***Abstract*—Transformer white-box models are used by the manufacturers to calculate internal winding voltages during the lightning impulse test. The model can also be applied in general network studies, but the model accuracy should then be improved, considering the many different voltage waveforms and frequencies that can exist in the system. Accuracy improvements are achievable by including the frequency-dependency of the branch impedance matrix via rational function approximation, but the large size of the matrix makes such modeling very difficult. Two suitable methods for passive rational modeling are presented, based on vector fitting and residue perturbation in either phase domain or modal domain. Application to a power transformer shows that the two methods are capable of fitting a 213×213 branch impedance matrix with a 6th order passive pole-residue model in a few seconds. The resulting model is included in a complete white-box state-space model of the transformer that is compatible with a previously implemented model interface for EMTP. An efficient procedure is presented for validating the simulation result by the Numerical Laplace Transform. Comparison with a measurement shows that the inclusion of the frequency dependency gives a better reproduction of the measured waveshape than a previously proposed damping-factor model.**

***Index Terms*—Transformer, white-box model, branch impedance, rational approximation, NLT, EMTP, simulation.**

I. Introduction

TRANSFORMER white-box models permit to calculate the internal voltages along the windings that result from transient voltages and currents on the external terminals [1], [2], [3], [4]. Such models are used by the transformer manufacturers to ensure that the windings will withstand the dielectric stresses that occur during the routine lightning impulse test in factory [4]. This type of model can also be used in general overvoltage studies with the transformer being part of a network, thereby enabling to calculate the internal voltages that can occur for a transformer in service, as well as the transfer of overvoltages between windings. The applied models are normally lumped-circuit representations that are calculated by considering a spatial discretization of the windings, defined by matrices of branch resistance $\mathbf{R}_B$ and inductance $\mathbf{L}_B$, and shunt capacitance **C** and conductance **G** [5]. Such models can be formulated on state-space diagonal form and be directly interfaced with EMT programs as shown in [6] and [7], or via a black-box modeling approach [8]. An alternative approach is to interface the model via a large, equivalent electrical circuit representation [9].

The maximum winding stresses during the lightning impulse test can often be calculated with sufficient accuracy without taking into account frequency-dependent damping effects in $\mathbf{R}_B$ and $\mathbf{L}_B$. These daily-use models have the advantage that the model parameters can be calculated very efficiently using analytical formulae [5]. The losses can, as a first approximation, be included by calculating the branch impedance resistance matrix $\mathbf{R}_B$ at a fixed frequency, giving a *k*-factor model [6]. It has been found [5], [10] that the daily-use models often have accuracy shortcomings when applied in general transient studies, in particular if one wishes to simulate the internal voltages that can occur in resonant situations, e.g. when the transformer is connected to a feeding cable that is subjected to energization. A more realistic loss representation can be achieved using the damping factor method (*d*-factor) [11], [12] which employs an empirical, frequency-dependent damping factor for modifying the eigenvalues of the state matrix of the white-box state-space model. That model, which is highly efficient in time domain simulations, can also properly represent the transformer behavior at the operating frequency [12], which is essential when initial 50/60 Hz initial conditions must be included in the simulation. A disadvantage is that the assumed damping curve is only an approximation to the actual damping of the transformer's natural frequencies.

For more accurate modeling, Finite Element Method (FEM) calculations can be used for obtaining branch impedance and shunt capacitance, at the cost of lengthy computations [5], [13]. The FEM calculations result in a frequency-dependent branch impedance matrix, $\mathbf{Z}_B(s) = \mathbf{R}_B(s) + s\mathbf{L}_B(s)$, $s = j\omega$. Such impedance matrix can be subjected to state-space modeling via a passive rational function approximation, and be introduced in

Manuscript received December 8, 2022,…

B. Gustavsen is with SINTEF Energy Research, N-7465 Trondheim, Norway (e-mail: bjorn.gustavsen@sintef.no).

This work was supported by Northwind (Norwegian Research Centre on Wind Energy), www.northwindresearch.no.

the *k*-factor model, leading to a complete frequency-dependent state-space model of the transformer [14]. The procedure in [14] achieves this by fitting a pole-residue model approximation to $\mathbf{Z}_B(s)$ by vector fitting (VF) [15]. Passivity is ensured by a modification to the model by enforcing positive definiteness for a set of matrices obtained from the rational model of $\mathbf{Z}_B(s)$, using particle swarm optimization.

The present work introduces two alternative approaches to the one in [14] which are conceptually simpler and more efficient. The first one fits a pole-residue model to $\mathbf{Z}_B$ in the phase domain, using poles that are obtained by fitting approximate eigenvalues using a common pole set. Passivity of the model is enforced in the phase domain by calculating a minimal perturbation with use of the RP-NNLS method [16], [17] which is capable of handling the large size of $\mathbf{Z}_B$. The second approach is based on approximate diagonalization of $\mathbf{Z}_B$ using a real, orthogonal transformation matrix. The rational fitting and passivity enforcement is performed for each diagonal element independently, leading to a highly efficient procedure that can utilize commonly available methods for the passivity enforcement, e.g. residue perturbation [18].

The rational model of $\mathbf{Z}_B$ by any of the two approaches gives, together with $\mathbf{G}$ and $\mathbf{C}$, a complete state-space model of the transformer that is cast on diagonal form for high computational performance in the time domain. The model is included in EMTP via the model interface for the *d*-factor model described in [7]. An efficient procedure is presented for validating the final model by comparing simulated responses against an alternative result by the inverse Numerical Laplace Transform (NLT) [19]. A comparison with the *d*-factor model and measurements is also provided, demonstrating the accuracy advantages of the proposed modeling.

All calculations are performed on a 64-bit Windows 10 laptop with 16 GB RAM and an Intel i7-76000U @2.8 GHz CPU. Matlab is used in the frequency domain calculations.

II. Transformer Modeling And Scope of Work

A. Overview

White-box transformer modeling for use in EMT simulation programs is a very comprehensive and arduous task. Fig. 1 gives an overview of the main steps in such procedure, with steps 3 and 5 being the technical contributions in this work.

1. *Detailed design data*. In this work, the transformer design data (geometry and material properties) are for a 1-ph 3-winding transformer (Section IV), provided by WEG Transformers, via CIGRE JWG A2/C4.52.
2. *FEM calculations.* Based on the design data, circuit parameters are calculated for the winding parts using suitable solvers for the governing field equations. The parameters are matrices of shunt conductance $\mathbf{G}$, shunt capacitance $\mathbf{C}$, and branch impedance $\mathbf{Z}_B(s)$ as function of discrete frequency. Details regarding the parameters used in this work are provided in Section IV.
3. *Rational approximation of* $\mathbf{Z}_B(s)$. The branch impedance matrix $\mathbf{Z}_B(s)$ is fitted with a stable and passive pole-residue model. Two alternative methods are proposed as described in Sections V and VI.
4. *State-space modeling of complete transformer*. The rational model $\mathbf{Z}_B$ is combined with $\mathbf{G}$ and $\mathbf{C}$ to obtain a complete state space model of the transformer (Section III.C).
5. *Validation.* The accuracy of steps 3 and 4 is validated in the frequency domain and time domain via nodal analysis and NLT, using data sets calculated from $\mathbf{G}$, $\mathbf{C}$ and $\mathbf{Z}_B(s)$ (Section VII).
6. *Model parameter data file.* The model parameters are written to ASCII file in a format proposed by CIGRE JWG A2/C4.52 [20].
7. *Model interface*. The state space model is included in a circuit simulator (EMTP) using the interface in [7].

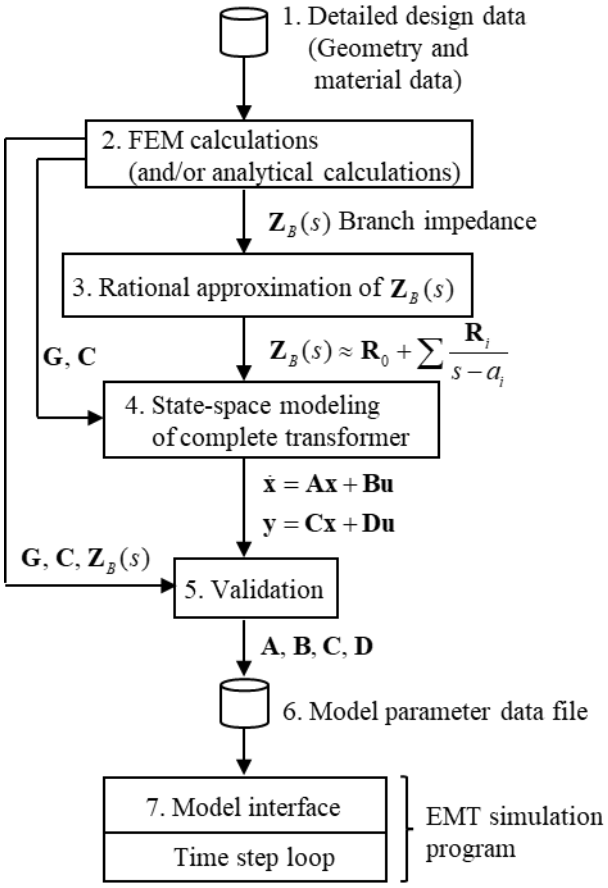

Fig. 1. Transformer white-box modeling and inclusion in EMT program.

B. Problem Statement

Consider a lumped parameter transformer representation, obtained by step 1 in Fig. 1. The data has N nodes and M mutually coupled impedance branches. The number of nodes and branches are high, typically several hundred. The parameters are the matrices of shunt conductance $\mathbf{G}^{N\times N}$, shunt capacitance $\mathbf{C}^{N\times N}$, and branch impedance $\mathbf{Z}_B^{M\times M}(s)$ given at K discrete frequency samples $s_k = j\omega_k$ (1). The parameters can come from analytical calculations and/or FEM calculations.

$$\mathbf{Z}_B(s_k) = \mathbf{R}_B(s_k) + s\mathbf{L}_B(s_k) \ , k = 1, 2, \ldots K \tag{1}$$

The objective is to include the frequency dependency in $\mathbf{Z}_B$ in a complete state-space model of the transformer (step 4 in Fig. 1), by calculating a low-order, passive rational function approximation (model) to the data (step 3). The rational fitting procedure is required to be computationally efficient, due to the large size $(M \times M)$ of $\mathbf{Z}_B$. The complete state-space model of the transformer is to be cast on diagonal form with real-valued and complex-conjugate parameters for efficient time domain simulations (step 6). A procedure for model validation is to be provided (step 5).

C. Symbols

Matrix: bold, capital letter.
Vector: bold, non-capital letter.
Scalar: non-bold, non-capital letter.

III. State-Space Modeling For Inclusion in EMT Programs

A. Circuit Equations

The following explains the establishing of the governing circuit equations, which form the basis for the transformer model to be developed.

Let $\mathbf{v}^{N\times 1}$, . $\mathbf{i}_B^{M\times 1}$., and $\mathbf{e}_B^{M\times 1}$ denote node voltages, inductive branch currents, and inductive branch voltages. These variables define the governing circuit equations by (2), (3), and (4).

$$\mathbf{i}_C(s) = s\mathbf{C}\mathbf{v}(s) \tag{2}$$

$$\mathbf{i}_G(s) = \mathbf{G}\mathbf{v}(s) \tag{3}$$

$$\mathbf{e}_B(s) = \mathbf{Z}_B(s)\mathbf{i}_B(s) \tag{4}$$

Kirchoff's current equation defines

$$\mathbf{i}_C + \mathbf{i}_L + \mathbf{i}_G = \mathbf{i}_S \tag{5}$$

where $\mathbf{i}_S^{N\times 1}$ are current injections from ground to the nodes, and $\mathbf{i}_L$ are currents associated with the branch impedances. The relation between node variables and inductive branch variables is given by the incidence matrix $\mathbf{T}^{M\times N}$ in (6) and (7).

$$\mathbf{e}_B = \mathbf{T}\mathbf{v} \tag{6}$$

$$\mathbf{i}_L = \mathbf{T}^T\mathbf{i}_B \tag{7}$$

The internal connections and groundings are handled by a modification to the matrices of $\mathbf{G}$, $\mathbf{C}$, and $\mathbf{T}$ as described in Appendix B of [6].

B. Illustrative Example

To see how the equations (2)-(7) relates to an equivalent circuit, consider as an example a two-winding transformer where each winding is divided into two branches. Fig. 2 shows the subdivision of the windings, giving a representation with *N*=6 nodes and *M*=4 inductive branches.

Fig. 3 shows the equivalent electric circuit. In addition, there exists mutual inductive couplings between all inductors (not shown). The 6×6 **C**-matrix is established from the partial capacitances, while in this case $\mathbf{G} = \mathbf{0}$. The branch impedance matrix $\mathbf{Z}_B$ is a 4×4 matrix whose diagonal elements are the elements $R_{ii} + j\omega L_{ii}$, in addition to the off-diagonal elements that represent the mutual coupling between the four *R-L* branches. The **T**-matrix, which relates node voltages to (inductive) branch voltages, is

$$\mathbf{T} = \begin{bmatrix} 1 & -1 & 0 & 0 & 0 & 0 \\ 0 & 1 & -1 & 0 & 0 & 0 \\ 0 & 0 & 0 & 1 & -1 & 0 \\ 0 & 0 & 0 & 0 & 1 & -1 \end{bmatrix} \tag{8}$$

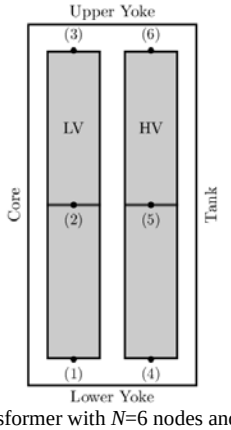

Fig. 2. Two-winding transformer with *N*=6 nodes and *M*=4 inductive branches [6].

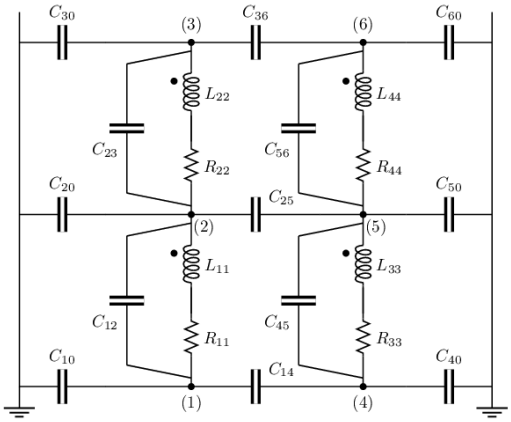

Fig. 3. Equivalent circuit of transformer in Fig. 2 [6].

C. State-Space Modeling

Inserting (2), (3) and (7) in (5) gives

$$\mathbf{G}\mathbf{v} + s\mathbf{C}\mathbf{v} + \mathbf{T}^T\mathbf{i}_B = \mathbf{i}_S \tag{9}$$

which can be rewritten as

$$s\mathbf{v} = -\mathbf{C}^{-1}\mathbf{G}\mathbf{v} - \mathbf{C}^{-1}\mathbf{T}^T\mathbf{i}_B + \mathbf{C}^{-1}\mathbf{i}_S \tag{10}$$

The branch current $\mathbf{i}_B$ is expressed as the output of an applied nodal voltage $\mathbf{v}$,

$$\mathbf{i}_B = \mathbf{Z}_B^{-1}\mathbf{e}_B = \mathbf{Z}_B^{-1}\mathbf{T}\mathbf{v} \tag{11}$$

Consider that a state-space model has been fitted to the branch admittance . $\mathbf{Y}_B = \mathbf{Z}_B^{-1}$. in (11),

$$s\mathbf{x}_Y = \mathbf{A}_Y\mathbf{x}_Y + \mathbf{B}_Y\mathbf{e}_B \tag{12a}$$

$$\mathbf{i}_B = \mathbf{C}_Y\mathbf{x}_Y + \mathbf{D}_Y\mathbf{e}_B \tag{12b}$$

Introducing (12b) in (10) gives

$$s\mathbf{v} = -\mathbf{C}^{-1}\mathbf{G}\mathbf{v} - \mathbf{C}^{-1}\mathbf{T}^T(\mathbf{C}_Y\mathbf{x}_Y + \mathbf{D}_Y\mathbf{T}\mathbf{v}) + \mathbf{C}^{-1}\mathbf{i}_S \tag{13}$$

Eq. (13) and (11a) are combined into a single state-space equation (14a) [14]. The output is given by (14b) where (12b) has been used for the lower partitioning.

$$s\begin{bmatrix}\mathbf{v}\\ \hline \mathbf{x}_Y\end{bmatrix} = \left[\begin{array}{c|c} -\mathbf{C}^{-1}(\mathbf{G}+\mathbf{T}^T\mathbf{D}_Y\mathbf{T}) & -\mathbf{C}^{-1}\mathbf{T}^T\mathbf{C}_Y \\ \hline \mathbf{B}_Y\mathbf{T} & \mathbf{A}_Y \end{array}\right]\cdot\begin{bmatrix}\mathbf{v}\\ \hline \mathbf{x}_Y\end{bmatrix} + \left[\begin{array}{c|c} \mathbf{C}^{-1} & \mathbf{0} \\ \hline \mathbf{0} & \mathbf{0} \end{array}\right]\cdot\begin{bmatrix}\mathbf{i}_S\\ \hline \mathbf{0}\end{bmatrix} \tag{14a}$$

$$\begin{bmatrix}\mathbf{v}\\ \hline \mathbf{i}_B\end{bmatrix} = \left[\begin{array}{c|c} \mathbf{I} & \mathbf{0} \\ \hline \mathbf{D}_Y\mathbf{T} & \mathbf{C}_Y \end{array}\right]\begin{bmatrix}\mathbf{v}\\ \hline \mathbf{x}_Y\end{bmatrix} \tag{14b}$$

The actual calculation of $\mathbf{A}_Y$, $\mathbf{B}_Y$, $\mathbf{C}_Y$, and $\mathbf{D}_Y$ is shown in Section V (phase domain fitting) and Section VI (modal domain fitting).

It is assumed that a node reordering has been made so that the external nodes come first. Such reordering is conveniently achieved using a node-reordering matrix [6]. The current injections now take place at the first (few) external nodes, $\mathbf{i}_S = [\mathbf{i}_{\text{ext}}^T \quad \mathbf{0}^T]^T$. In the time domain one can now write for (14),

$$\begin{bmatrix}\dot{\mathbf{v}}_{\text{ext}}\\ \dot{\mathbf{v}}_{\text{int}}\\ \dot{\mathbf{x}}_Y\end{bmatrix} = \begin{bmatrix}\mathbf{A}_1 & \mathbf{A}_2 & \mathbf{A}_3\end{bmatrix}\cdot\begin{bmatrix}\mathbf{v}_{\text{ext}}\\ \mathbf{v}_{\text{int}}\\ \mathbf{x}_Y\end{bmatrix} + \begin{bmatrix}\mathbf{B}_1 & \mathbf{B}_2 & \mathbf{B}_3\end{bmatrix}\cdot\begin{bmatrix}\mathbf{i}_{\text{ext}}\\ \mathbf{0}\\ \mathbf{0}\end{bmatrix} \tag{15a}$$

$$\begin{bmatrix}\mathbf{v}_{\text{ext}}\\ \mathbf{v}_{\text{int}}\\ \hline \mathbf{i}_B\end{bmatrix} = \left[\begin{array}{c|c|c} \mathbf{I}_{\text{ext}} & & \\ & \mathbf{I}_{\text{int}} & \mathbf{0} \\ \hline \mathbf{D}_Y\mathbf{T} & & \mathbf{C}_Y \end{array}\right]\cdot\begin{bmatrix}\mathbf{v}_{\text{ext}}\\ \mathbf{v}_{\text{int}}\\ \hline \mathbf{x}_Y\end{bmatrix} \tag{15b}$$

One is usually not interested in the branch currents $\mathbf{i}_B$, implying that the lower partition of the output part in (15b) can be omitted from the model.

This work will further take advantage of the implemented EMTP model interface [7] for the *d*-factor model, which assumes voltage on external terminals as input. With that approach, small resistors are introduced in series with the external terminals, permitting to write (15) with voltage on external terminals as input [12]. Subjecting the resulting state matrix to diagonalization gives the final result (16), where $\mathbf{A}$ is diagonal. The output matrices $\mathbf{C}_1$ and $\mathbf{C}_2$ are full. The steps for going from (15) to (16) are shown in detail in Section III.C in [12].

$$\dot{\mathbf{x}} = \mathbf{A}\mathbf{x} + \mathbf{B}\mathbf{v}_{\text{ext}} \tag{16a}$$

$$\mathbf{i}_{\text{ext}} = \mathbf{C}_1\mathbf{x} + \mathbf{D}_1\mathbf{v}_{\text{ext}} \tag{16b}$$

$$\mathbf{v}_{\text{int}} = \mathbf{C}_2\mathbf{x} \tag{16c}$$

D. Calculation Routines

All calculations are performed using Matlab R2018b, with rational fitting based on vector fitting (VF) implementations downloadable from a web site [21]. For passivity enforcement of $\mathbf{Z}_B$ in the phase domain (Section V), a separate Matlab implementation is used which realizes the RP-NLLS method described in [16] (not available on web site). For passivity enforcement of $\mathbf{Z}_B$ in the modal domain (Section VI), the web site routine RPdriver.m is used.

IV. Example: Single-Phase Transformer

The methods presented in this work are applied to a 1-ph 3-winding transformer, see Fig. 4. It is a 50 MVA unit with rated voltage $230/\sqrt{3}$, $69/\sqrt{3}$, 13.8 kV at 60 Hz. This transformer has been extensively studied and modeled in CIGRE JWG A2/C4.52. Detailed design information is given in [10].

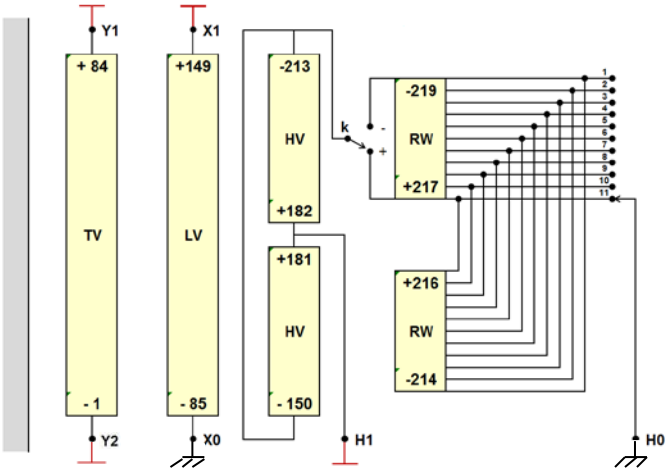

Fig. 4. Single phase transformer with external terminals (H1-181/182, X1-149, Y1-84, Y2-1) and internal nodes.

Lumped model parameters have been calculated for this transformer, for a discretization with *N*=219 nodes and *M*=213 coupled impedance branches. The parameter set was provided by Prof. Enrique Mombello, Universidad Nacional de San Juan, Argentina. It consists of the capacitance matrix $\mathbf{C}^{219\times219}$ and the branch impedance $\mathbf{Z}_B^{213\times213}(\omega)$ at *K*=18 logarithmically spaced frequencies in the range 50 Hz-1 MHz. The data set, which was calculated by FEM, was shown in [14] to give a high accuracy for representing the transformer in transient calculations.

V. Phase Domain Branch Impedance Modeling

A. Rational Fitting

The discrete data set for $\mathbf{Z}_B$ in (1) is in the following denoted as $\mathbf{Z}_B^{\text{data}}$, to distinguish it from the frequency response of its rational model approximation that is to be calculated.

The large size of $\mathbf{Z}_B^{\text{data}}$ ($M > 100$) can make its direct fitting by a common pole set time consuming, even with the use of the

fast implementation [22] of VF. Fortunately, the smooth behavior permits the use of a low-order rational approximation. The computational efficiency is greatly improved by obtaining the common pole set by fitting approximate eigenvalues of $\mathbf{Z}_B^{\text{data}}$, rather than the full matrix.

The given matrix $\mathbf{Z}_B^{\text{data}}$ is subjected to diagonalization by eigenvector decomposition at one of the given frequencies, s_0, in the data set.

$$\mathbf{Z}_B^{\text{data}}(s_0) = \mathbf{T}_Z\ \boldsymbol{\Gamma}_Z\ \mathbf{T}_Z^{-1} \tag{17}$$

The obtained transformation matrix $\mathbf{T}_Z$ is replaced by a real transformation matrix $\bar{\mathbf{T}}_Z$. This is achieved by rotating the eigenvectors $(\mathbf{t}_{Z,i} \rightarrow \xi_i \mathbf{t}_{Z,i}, |\xi_i| = 1)$ to minimize their imaginary part in the least squares sense, followed by removal of their imaginary part [23]. The approach is described in Appendix C.15.1 in [24]. The resulting transformation matrix $\bar{\mathbf{T}}_Z$ is assumed to apply at all frequencies, and it is used for calculating approximate eigenvalues by (18).

$$\boldsymbol{\lambda}_Z(s) \approx \boldsymbol{\lambda}'_Z(s) = diag(\bar{\mathbf{T}}_Z^{-1}\mathbf{Z}_B^{\text{data}}(s)\bar{\mathbf{T}}_Z) \tag{18}$$

The (approximate) eigenvalues (18) are stacked in a single vector and fitted by a common pole set (19) using VF with enforcement of stable, real-valued poles. Any complex conjugate pair is replaced with two close, real poles [25].

$$\boldsymbol{\lambda}'_Z(\omega) \approx \mathbf{r}_0^Z + \sum_{i=1}^{P_Z} \frac{\mathbf{r}_i^Z}{s - p_i^Z} \tag{19}$$

Finally, the original matrix $\mathbf{Z}_B^{\text{data}}$ is fitted in the phase domain with known poles . p_i^Z , $i = 1,\ldots P_Z$., giving the unknown residue matrices $\mathbf{R}_i^Z$, $i = 1,\ldots P_Z$ (20). The resulting model is reciprocal with real-valued poles and residue matrices.

$$\mathbf{Z}_B^{\text{data}}(s) \approx \mathbf{Z}_B(s) = \mathbf{R}_0^Z + \sum_{i=1}^{P_Z} \frac{\mathbf{R}_i^Z}{s - p_i^Z} \tag{20}$$

Fig. 5 shows the first column of a 6th order rational approximation of $\mathbf{Z}_B^{\text{data}}$, using a $\bar{\mathbf{T}}_Z$ calculated at 10 kHz. Five VF iterations were used. The model reproduces the data with good accuracy. The final poles are listed in Table I.

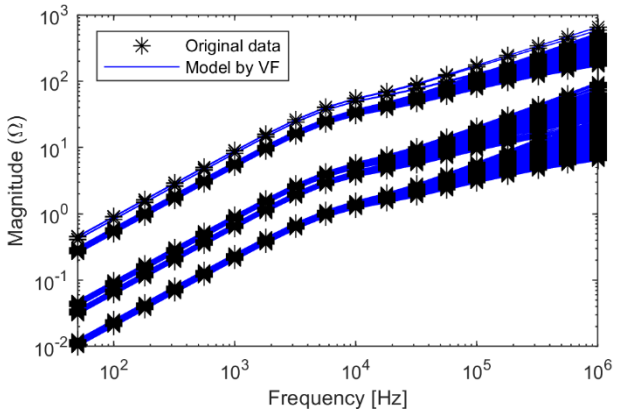

Fig. 5. Elements in first column of $\mathbf{Z}_B(\omega)$. Original data and 6th order rational approximation. M=213 elements in plot.

TABLE I
POLES USED IN THE FITTING OF $\mathbf{Z}_B(s)$.

-5.6647E+03	-4.3769E+04	-4.1081E+05
-1.6365E+06	-7.3183E+06	-1.5856E+08

B. *Passivity Enforcement*

Passivity of the model (20) must be enforced to ensure stable time domain simulations. The enforcement is achieved by perturbing the model's residue matrices such that the fitted matrix $\mathbf{Z}_B$ satisfies the positive eigenvalues condition (21) for all frequencies [24]. Superscript ^{H} denotes Hermite (transpose and conjugate).

$$\mathbf{Z}_B(s) + \mathbf{Z}_B^H(s) > 0\ \forall s \tag{21}$$

The large size M of $\mathbf{Z}_B$ makes it impossible to directly apply commonly used methods, such as residue perturbation [18] or residue matrix eigenvalue perturbation [26]. Those methods require to iteratively solve a large, constrained least squares problem. The size difficulty is overcome by usage of the (iterative) RP-NNLS method [16], [17] which by QR-decomposition gives a compacted, non-negative least squares problem to be solved.

Passivity is enforced by RP-NNLS with sweeping over 200 frequency samples for the passivity assessment. Fig. 6 shows the result of the passivity on the (real-valued) eigenvalues of $\mathbf{Z}_B(s) + \mathbf{Z}_B^H(s)$. It is observed that the passivity enforcement results in that all eigenvalues become positive. A single iteration by RP-NNLS was needed.

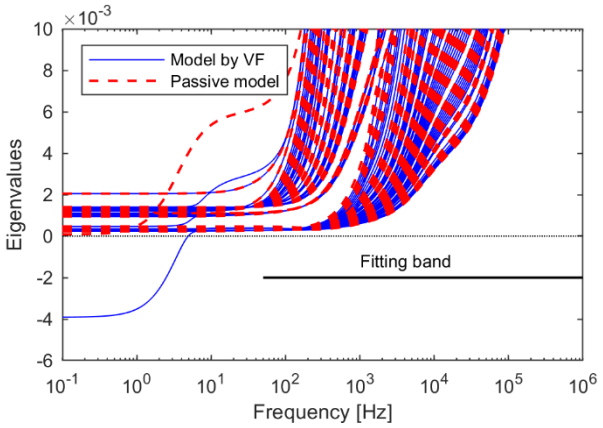

Fig. 6. Impact of passivity enforcement on eigenvalues of $\mathbf{Z}_B(s)+\mathbf{Z}_B^H(s)$.

Fig. 7 shows the magnitude of the (exact) eigenvalues of $\mathbf{Z}_B^{\text{data}}$ in the fitting range. Also is shown the (exact) eigenvalues of the passive model $\mathbf{Z}_B$ and of the non-passive model. It is observed that the passive model gives a very accurate representation of the original data and that the passivity enforcement does not lead to any observable change in the eigenvalues. This result implies that also all elements of $\mathbf{Z}_B$ are accurately represented, which can be observed for the first column of $\mathbf{Z}_B$ in Fig. 8. A zoomed view of the plot revealed negligible deviations.

Table II summarizes the CPU time for the rational fitting and passivity enforcement. The entire modeling required 12.8 sec.

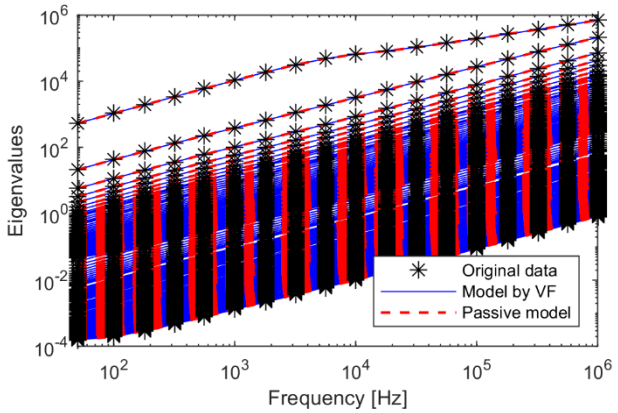

Fig. 7. Eigenvalues of $\mathbf{Z}_B(s)$.

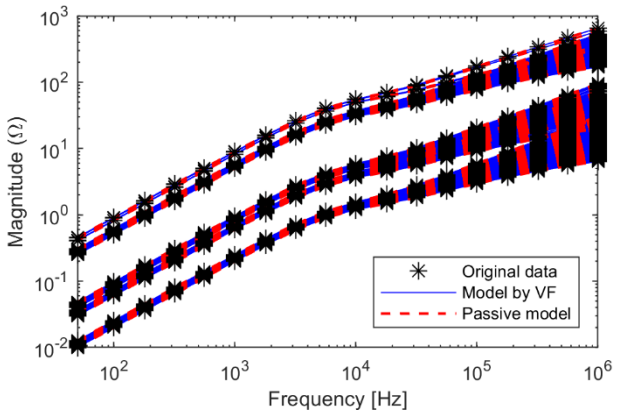

Fig. 8. First column of $\mathbf{Z}_B(s)$. Phase domain model.

TABLE II
COMPUTATION TIME FOR EXTRACTING PHASE DOMAIN MODEL OF $\mathbf{Z}_B(s)$.

RATIONAL APPROXIMATION	PASSIVITY CHECKING	PASSIVITY ENFORCEMENT	**TOTAL**
8.6 SEC	2.0 SEC	2.2 SEC	**12.8 SEC**

C. Least Squares Weighting

The passivity violations that can occur are strongly dependent on the least squares (LS) weighting scheme adopted in the rational fitting and passivity enforcement steps. The following frequency-dependent weighting scheme (22a), (22b), (22c) was successfully adopted in this work. 1) Calculate poles by (19) using inverse vector norm weighting w_1; 2) calculate residue matrices by (20) using inverse element magnitude weighting w_2; 3) enforce passivity using inverse matrix norm weighting w_3. The proposed weighting scheme gave small passivity violations for all relevant model orders, from 4 to 10.

$$w_1(s)=\frac{1}{\|\boldsymbol{\lambda}'_Z(s)\|} \tag{22a}$$

$$w_{2,i,j}(s)=\frac{1}{\|Y_{B,i,j}(s)\|}\ ,\ i=1\ldots M,\ j=1\ldots M \tag{22b}$$

$$w_3(s)=\frac{1}{\|\mathbf{Y}_B(s)\|} \tag{22c}$$

D. Conversion to Branch Admittance Model

The passive pole-residue model (20) is converted into a state-space model (23) [27],

$$\mathbf{Z}_B=\mathbf{C}_Z(s\mathbf{I}-\mathbf{A}_Z)^{-1}\mathbf{B}_Z+\mathbf{D}_Z \tag{23}$$

A state-space model for the branch *admittance* matrix $\mathbf{Y}_B$ is obtained by exchanging the model's input and output, [24]. The conversion (24) with parameters (25) required 0.03 sec. The matrix sizes are given in Table III.

$$\mathbf{Y}_b=\mathbf{C}_Y(s\mathbf{I}-\mathbf{A}_Y)^{-1}\mathbf{B}_Y+\mathbf{D}_Y \tag{24}$$

$$\left[\begin{array}{c|c}\mathbf{A}_Y & \mathbf{B}_Y\\ \hline \mathbf{C}_Y & \mathbf{D}_Y\end{array}\right]=\left[\begin{array}{c|c}\mathbf{A}_Z-\mathbf{B}_Z\mathbf{D}_Z^{-1}\mathbf{C}_Z & -\mathbf{B}_Z\mathbf{D}_Z^{-1}\\ \hline \mathbf{D}_Z^{-1}\mathbf{C}_Z & \mathbf{D}_Z^{-1}\end{array}\right] \tag{25}$$

TABLE III
MATRIX SIZES OF BRANCH ADMITTANCE MODEL.

$\mathbf{A}_Y$	$\mathbf{B}_Y$	$\mathbf{C}_Y$	$\mathbf{D}_Y$
$P_Z M\times P_Z M$	$P_Z M\times M$	$M\times P_Z M$	$M\times M$

VI. MODAL DOMAIN BRANCH IMPEDANCE MODELING

The following describes an alternative modeling variant which is based on diagonalization. The rational modeling and passivity enforcement is now applied to scalar functions rather than (large) matrix functions, thereby avoiding the need for RP-NNLS and the potentially long calculation times and robustness issues associated with passivity violations.

A. Diagonalization Using Orthogonal Matrix

The branch admittance matrix $\mathbf{Y}_B=\mathbf{Z}_B^{-1}$ is calculated at a

user-defined frequency s_0 that is considered representative for the transient analysis. Eigenvector decomposition is applied to $\mathbf{Y}_B(s_0)$,

$$\mathbf{Y}_B(s_0) = \mathbf{T}_Y\ \mathbf{\Gamma}_Y\ \mathbf{T}_Y^{-1} \tag{26}$$

where $\mathbf{\Gamma}_Y$ is a diagonal matrix holding the eigenvalues of $\mathbf{Y}_B(s_0)$. The eigenvector matrix $\mathbf{T}_Y$ is in general complex. It is replaced with an approximate eigenvector matrix $\mathbf{T}_Y \approx \mathbf{T}_{\text{Re}}$ by rotating each eigenvector to minimize its imaginary part [23], [24] and retaining only the real part. The use of this approximate (real) matrix $\mathbf{T}_{\text{Re}}$ does *not* give a symmetrical matrix (unlike the original $\mathbf{T}$), i.e. for any diagonal matrix $\mathbf{\Gamma}$,

$$\mathbf{T}_{\text{Re}}\ \mathbf{\Gamma}\ \mathbf{T}_{\text{Re}}^{-1} \neq (\mathbf{T}_{\text{Re}}\ \mathbf{\Gamma}\ \mathbf{T}_{\text{Re}}^{-1})^T \tag{27}$$

To achieve symmetry for (27), $\mathbf{T}_{\text{Re}}$ is replaced with a (real) *orthogonal* approximation matrix $\mathbf{T}_{\text{O}}$. A suitable orthogonal $\mathbf{T}_{\text{O}}$ is calculated via the singular value decomposition $\mathbf{T}_{\text{Re}} = \mathbf{U}_{\text{Re}}\mathbf{\Sigma}_{\text{Re}}\mathbf{V}_{\text{Re}}^H$ which by (28) gives the closest possible orthogonal matrix in the least squares sense [28].

$$\mathbf{T}_{\text{O}} = \mathbf{U}_{\text{Re}}\mathbf{V}_{\text{Re}}^H \tag{28}$$

The orthogonality property implies $\mathbf{T}_{\text{O}}^{-1} = \mathbf{T}_{\text{O}}^T$ so that the symmetry (29) holds with any diagonal matrix $\mathbf{\Gamma}$.

$$\mathbf{T}_{\text{O}}\ \mathbf{\Gamma}\ \mathbf{T}_{\text{O}}^{-1} = (\mathbf{T}_{\text{O}}\ \mathbf{\Gamma}\ \mathbf{T}_{\text{O}}^{-1})^T \tag{29}$$

The orthogonal $\mathbf{T}_{\text{O}}$ is applied as a similarity transformation to $\mathbf{Y}_B^{\text{data}}$, and the off-diagonal elements are discarded to give a diagonal matrix whose non-zero elements are stacked into a vector $\mathbf{y}'_B$,

$$\mathbf{y}'_B(s) = diag\{\mathbf{T}_{\mathbf{O}}^T\ \mathbf{Y}_B^{\text{data}}(s)\ \mathbf{T}_{\text{O}}\} \tag{30}$$

B. Rational Fitting

The elements $y'_{B,m}$ of $\mathbf{y}'_B$ are fitted independently by a pole-residue model (31) using VF with enforcement of stable, real poles, and subjected to passivity enforcement,

$$y'_{B,m}(s) \approx r_{0,m} + \sum_{i=1}^{P_{Y,m}} \frac{r_{i,m}}{s - p_{i,m}}\ ,\ m = 1 \ldots M \tag{31}$$

Fig. 9 shows 6th order rational approximations of the diagonal elements $y'_{B,m}(s)$ with $\mathbf{T}_{\text{O}}$ calculated at the mid-band frequency (11 kHz). The fitting by VF used five iterations with inverse magnitude weighting. Passivity was assessed using a half-size test matrix [29]. No passivity enforcement was needed in this case. It is observed that all diagonal elements have been accurately fitted.

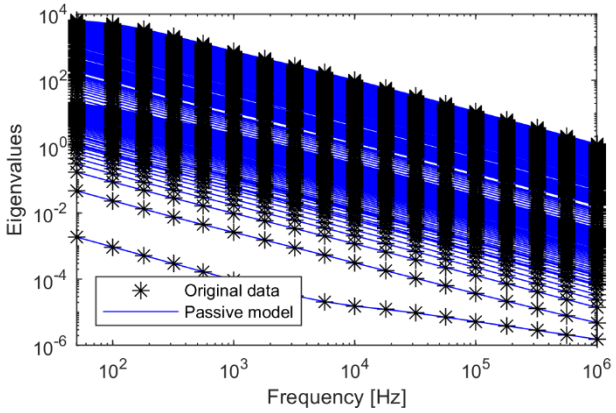

Fig. 9. Fitted diagonal elements $y'_{B,m}(s)$.

The scalar models (31) are expanded into state-space models (32) where $\mathbf{A}_m$ is a diagonal matrix that holds the poles $\{p_{i,m}\}$, $\mathbf{c}_m^T$ holds the residue elements $\{r_{i,m}\}$, $\mathbf{b}_m$ is a column of ones, $d_m = r_{0,m}$, and $\mathbf{I}_m$ is the (diagonal) identity matrix.

$$r_{0,m} + \sum_{i=1}^{P_{Y,m}} \frac{r_{i,m}}{s - p_{i,m}} \rightarrow \mathbf{c}_m^T(s\mathbf{I}_m - \mathbf{A}_m)^{-1}\mathbf{b}_m + d_m \tag{32}$$

The contribution $\mathbf{Y}_{B,m}$ to the complete state-space model is obtained by combining the rational approximation of $y'_{B,m}(\omega)$ with the corresponding column $\mathbf{t}_{\text{O},k}$ of $\mathbf{T}_{\text{O}}$,

$$\mathbf{Y}'_{B,m} \approx \mathbf{t}_{\text{O},m}(\mathbf{c}_m^T(j\omega\mathbf{I}_m - \mathbf{A}_m)^{-1}\mathbf{b}_m + d_m)\mathbf{t}_{\text{O},m}^T \tag{33}$$

The complete state-space model (24) is written by inspection, giving parameter matrices (34a) and (34b).

$$\mathbf{A}_Y = \begin{bmatrix} \mathbf{A}_1 & \mathbf{0} & \cdots & \mathbf{0} \\ \mathbf{0} & \mathbf{A}_2 & & \mathbf{0} \\ \vdots & \mathbf{0} & \ddots & \vdots \\ \mathbf{0} & \mathbf{0} & \cdots & \mathbf{A}_M \end{bmatrix},\ \mathbf{B}_Y = \begin{bmatrix} \mathbf{1} & \mathbf{0} & \cdots & \mathbf{0} \\ \mathbf{0} & \mathbf{1} & & \mathbf{0} \\ & \vdots & \ddots & \mathbf{0} \\ \mathbf{0} & \mathbf{0} & & \mathbf{1} \end{bmatrix}\mathbf{T}_{\text{O}}^T \tag{34a}$$

$$\mathbf{C}_Y = \mathbf{T}_{\text{O}}\begin{bmatrix} \mathbf{c}_1^T & \mathbf{0}^T & \cdots & \mathbf{0}^T \\ \mathbf{0}^T & \mathbf{c}_2^T & & \mathbf{0}^T \\ \vdots & & \ddots & \vdots \\ \mathbf{0}^T & \mathbf{0}^T & \cdots & \mathbf{c}_M^T \end{bmatrix},\ \mathbf{D}_Y = \mathbf{T}_{\text{O}}\begin{bmatrix} d_1 & 0 & \cdots & 0 \\ 0 & d_1 & & 0 \\ \vdots & & \ddots & \vdots \\ 0 & 0 & \cdots & d_M \end{bmatrix}\mathbf{T}_{\text{O}}^T \tag{34b}$$

The accuracy of the final model is assessed by comparing calculated samples $\mathbf{Z}_B = \mathbf{Y}_B^{-1}$ from the model against the original data samples $\mathbf{Z}_B^{\text{data}}$. The accuracy is found to be lower than for the phase domain model. This result is to be expected because the modal domain model assumes the transformation matrix $\mathbf{T}_{\text{O}}$ (28) to be valid at all frequencies, which is an approximation. The deviations are more easily observed in Fig. 10 which displays every 30th element of the first column of the inductance part $\mathbf{L}_B$ of the impedance matrix $\mathbf{Z}_B = \mathbf{R}_B + s\mathbf{L}_B$. The plot also includes the ditto result by the phase domain model, showing a higher accuracy.

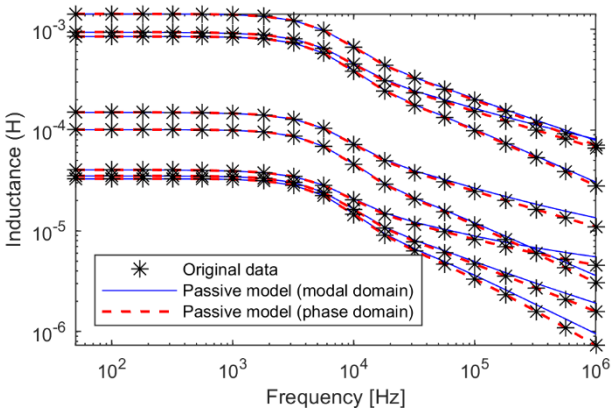

Fig. 10. Eight elements from first column of $\mathbf{L}_B(s)$.

Table IV shows the CPU time for the various steps in the modeling procedure. The total CPU time is about 3.7 sec, including the diagonalization, rational modeling, and the expansion to a complete state-space model by (34a) and (34b).

TABLE IV
COMPUTATION TIME FOR EXTRACTING MODAL DOMAIN MODEL OF $\mathbf{Y}_B(s)$.

VECTOR FITTING AND PASSIVITY ENFORCEMENT	OTHER	**TOTAL**
2.0 SEC	1.7 SEC	**3.7 SEC**

If one fits all of the M diagonal elements using P_Y poles, the size of the matrices become as shown in Table V. The matrix sizes are now the same as for the phase domain state-space model (20) if one uses the same model order, $P_Y = P_Z$.

TABLE V
MATRIX SIZES.

$\mathbf{A}_Y$	$\mathbf{B}_Y$	$\mathbf{C}_Y$	$\mathbf{D}_Y$
$P_Y M \times P_Y M$	$P_Y M \times M$	$M \times P_Y M$	$M \times M$

VII. MODEL VALIDATION

The complete, diagonalized white-box model (16a), (16b) and (16c) can potentially have errors due to inaccuracies in the rational fitting of $\mathbf{Z}_B$, the subsequent passivity enforcement, and the diagonalization. In what follows is presented an efficient model validation procedure for use in both frequency domain and time domain. The steps can be summarized as follows.

1. Fit the elements of $\mathbf{Z}_B$ using a sufficiently high order, such that all elements are fitted with high relative accuracy. Passivity is not enforced. Denote this model $\bar{\mathbf{Z}}_B$.
2. Using the "accurate" rational model $\bar{\mathbf{Z}}_B$, calculate frequency samples in the Laplace domain $(s = \sigma + j\omega)$ for the $N \times N$ nodal admittance matrix $\mathbf{Y}(s)$. With the aid of $\mathbf{Y}(s)$, calculate voltage transfer functions between external terminals, and from external nodes to selected internal nodes [8].
3. Calculate the ditto voltage transfer quantities in the time domain using inverse Laplace Transform (NLT) [19].

The three steps are described in the following subsections.

A. Calculate Alternative Rational Model $\bar{\mathbf{Z}}_B$

The branch impedance $\mathbf{Z}_B^{\text{data}}$ is fitted in the phase domain using a higher order model to achieve improved accuracy. Passivity is not enforced. This rational model is used for calculating frequency samples in the left half plane $(s = \sigma + j\omega)$ on a linear base $\{j\omega_k\}$ with a suitable shift σ, giving $\bar{\mathbf{Z}}_B(s)$.

B. Calculate Transfer Functions in Laplace Domain

Inserting the inverse of (4) into (9) and introducing $\mathbf{e}_B = \mathbf{T}\mathbf{v}$ from (4) gives

$$\mathbf{G}\mathbf{v} + s\mathbf{C}\mathbf{v} + \mathbf{T}^T \mathbf{Y}_B(s)\mathbf{T}\mathbf{v} = \mathbf{i}_S \tag{35}$$

The full $N \times N$ admittance matrix $(\mathbf{Y}\mathbf{v} = \mathbf{i}_S)$ can now be calculated from (35) as

$$\mathbf{Y}(s) = \mathbf{G} + s\mathbf{C} + \mathbf{T}^T \mathbf{Y}_B(s)\mathbf{T} \tag{36}$$

Inverting the admittance matrix (36) gives

$$\mathbf{Z}(s) = \mathbf{Y}^{-1}(s) \tag{37}$$

Deleting all rows and columns of $\mathbf{Z}$ except for those corresponding to the external terminals gives a reduced-size matrix $\mathbf{Z}_{\text{ext}}$. Finally, the terminal admittance matrix is obtained by inverting $\mathbf{Z}_{\text{ext}}$,

$$\mathbf{Y}_{\text{ext}}(s) = \mathbf{Z}_{\text{ext}}^{-1}(s) \tag{38}$$

The voltage $\mathbf{v}_{\text{ext}}$ at external terminals can be assumed known or be calculated using nodal analysis. With $\mathbf{v}_{\text{ext}}$ known, the voltage at internal nodes is calculated via the full $\mathbf{Z}$. With the partitioning in (39), it follows from the condition $\mathbf{i}_{\text{int}} = \mathbf{0}$ that the internal voltages can be calculated by (40) [8].

$$\begin{bmatrix} \mathbf{v}_{\text{ext}} \\ \mathbf{v}_{\text{int}} \end{bmatrix} = \begin{bmatrix} \mathbf{Z}_A & \mathbf{Z}_B \\ \mathbf{Z}_C & \mathbf{Z}_D \end{bmatrix} \begin{bmatrix} \mathbf{i}_{\text{ext}} \\ \mathbf{i}_{\text{int}} \end{bmatrix} \tag{39}$$

$$\mathbf{v}_{\text{int}}(s) = \mathbf{Z}_C(s)\mathbf{Y}_{\text{ext}}(s)\mathbf{v}_{\text{ext}}(s) \tag{40}$$

Fig. 11 shows the calculated voltage transfer function from external terminal H1 to open terminal X1, when Y1 and Y2 are also open. It is observed that the frequency response is much smoother when evaluated along $s = \sigma + j\omega$ compared to the imaginary axis $s = j\omega$. The shift σ was chosen as [30]

$$\sigma = \frac{\ln(K^2)}{T} \tag{41}$$

where T is the upper time limit in the corresponding time domain response that is to be calculated (next subsection), and K is the number of frequency samples. This case used a value $\sigma = 8.54 \cdot 10^4$, corresponding to $T = 110\,\mu\text{s}$ and $K = 110$,

defining a time resolution of 1 µs. The K sample values to be used for NLT are shown by the dots.

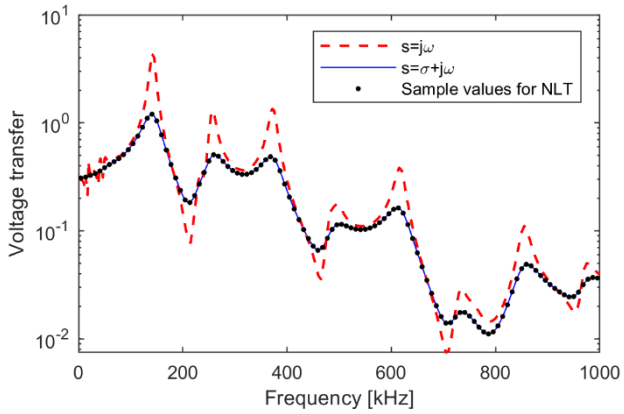

Fig. 11. Voltage transfer function from H1 to X1, evaluated at alternative frequency domain paths.

C. Calculate Validating Time Domain Responses by NLT

The K sample values are transformed to the time domain by the Fast Fourier Transform (FFT) where they are used for validating EMTP simulation results by the white-box model. This work uses an NLT implementation described in detail in [19]. The ten last samples are discarded due to lower accuracy.

Fig. 12 shows a validation example where a standard 1.2/50 µs lightning impulse voltage (42) is applied to terminal H1, with k=1.0383, a=0.015·10^6, b=2.47·10^6.

$$U(t) = k(e^{-at} - e^{-bt}) \tag{42}$$

The voltage response is calculated for (open) terminals X1, Y1, Y2 and two nodes (228, 219) in the regulating winding. In EMTP, the two alternative models (phase domain fitting, modal domain fitting) are employed with 5001 time steps ($\Delta t = 0.02$ µs). In the NLT validation, the corresponding lightning impulse responses are obtained by scaling each (impulse) response $F(s)$ from Section VII.B by a factor $g(s)$,

$$g(s) = \frac{k}{s+a} - \frac{k}{s+b} \tag{43}$$

An excellent agreement is observed between the NLT result (110 samples) and the simulation result by the two alternative EMTP models (5001 samples).

The CPU time for the NLT calculations is 12 sec with a 10th order rational model for $\mathbf{Z}_B$ and five VF iterations, see Table VI. The CPU time is identical for the two EMTP models (phase domain fitting or modal domain fitting of $\mathbf{Z}_B$) because the same model order ($P_Z = P_Y = 6$) was used. Therefore, the matrix sizes of the final model are the same. The CPU time for the EMTP simulation is given in Table VII for two situations: using the model as a four-node terminal equivalent, and when additionally simulating all (229-4=215) internal node voltages. The CPU time is 0.43 sec and 2.1 sec for the two cases.

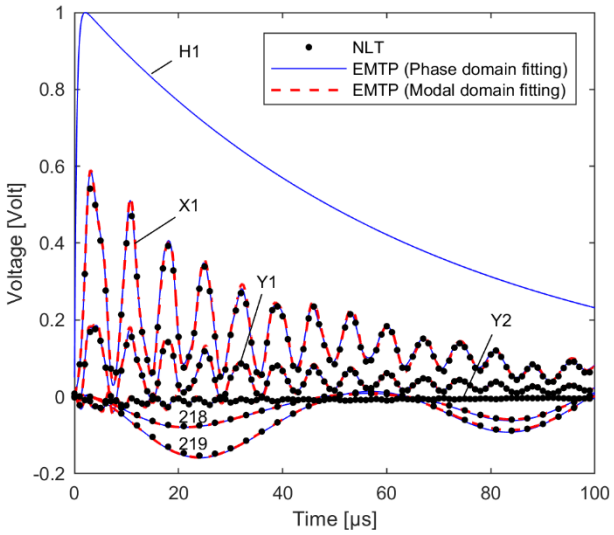

Fig. 12. Comparison between NLT result (110 sample values) and EMTP simulation (5001 sample values). Lightning impulse voltage transfer from HV terminal (H1) to open LV terminal (X1), tertiary terminals (Y1, Y2), and two nodes in regulating winding (228, 219).

TABLE VI
NLT COMPUTATION TIME (120 SAMPLES).

CALCULATING 110 SAMPLES FOR $\mathbf{Y}$ VIA RATIONAL FITTING OF $\mathbf{Z}_B$.	12 SEC
TRANSFORMING 110 SAMPLES TO TIME DOMAIN	0.003 SEC

TABLE VII
EMTP COMPUTATION TIME. 5000 TIME STEPS.

EXTERNAL VOLTAGES ONLY	0.43 SEC
EXTERNAL AND INTERNAL VOLTAGES	2.1 SEC

VIII. SENSITIVITY TO DIAGONALIZATION FREQUENCY

The calculations by the EMTP model with modal domain fitting of $\mathbf{Z}_B$ used a transformation matrix calculated at 10 kHz. As the transformation matrix is in reality frequency-dependent, one can expect that the simulated result will depend on the selected frequency for diagonalization.

Fig. 13 shows the same results as in Fig. 12, when using modal domain fitting with three alternative frequencies for diagonalization: 50 Hz, 10 kHz, and 1 MHz. It is observed that the responses are only weakly dependent on the chosen frequency for diagonalization.

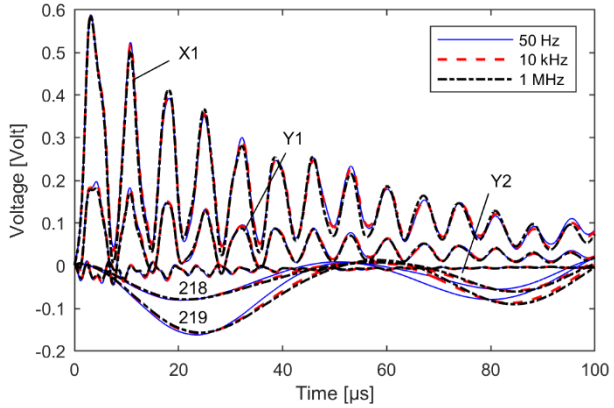

Fig. 13. Simulations with modal domain fitting of $\mathbf{Z}_B$, with alternative frequencies for diagonalization. Voltage response in X1, Y1, Y2, 218, 219.

IX. Comparison With Damping Factor Model

One alternative to the proposed model is the *d*-factor model which makes use on an empirical, frequency-dependent damping factor. The input parameters for that model are the lossless branch inductance matrix $\mathbf{L}_B^{\text{lossless}}$, in addition to the capacitance matrix $\mathbf{C}$. The state-space model (16a), (16b), (16c) is formulated in a similar manner as the one in this work. Finally, the real part of the (diagonal) state matrix elements are replaced according to the damping function, which defines the real part α as function of the imaginary part β.

A *d*-factor model was constructed from the data by taking as $\mathbf{L}_B$ the imaginary part of $\mathbf{Z}_B$ at the highest frequency sample (1 MHz). The model parameters were exported to file and included in EMTP using the same model interface as in the previous calculations. Fig. 14 compares the simulation result by the *d*-factor model with the model proposed in this work when using phase domain fitting of $\mathbf{Z}_B$. As damping factor was chosen the one proposed by Fergestad (44a), (44b) in his PhD thesis work [31], based on measurements on 25 transformers.

$$0 < \beta < 0.5\cdot 10^6 \rightarrow \alpha = -(0.022\beta + 0.058\cdot 10^{-6}\beta^2) \quad (44a)$$

$$\beta > 0.5\cdot 10^6 \rightarrow \alpha = -0.05\beta \quad (44b)$$

It is observed that the *d*-factor model gives a stronger attenuation of the fast oscillation than the proposed model. The same plot also includes the associated measurement result provided by CIGRE JWG A2/C4.52 [10], by the following procedure [32]. 1) Voltage transfer function measurement in the frequency domain, 2) rational function approximation, and 3) time domain response calculation using convolution. The use of a full frequency-dependent $\mathbf{Z}_B$ gives a better agreement with the measurement. With the *d*-factor model, simulating external overvoltages (5000 time steps) required 0.21 sec (compared to 0.43 sec for proposed model), and including all internal overvoltages required 0.53 sec (compared to 2.1 sec for proposed model). The faster calculations are mainly a consequence of fewer columns in the state output matrix $\mathbf{C}$.

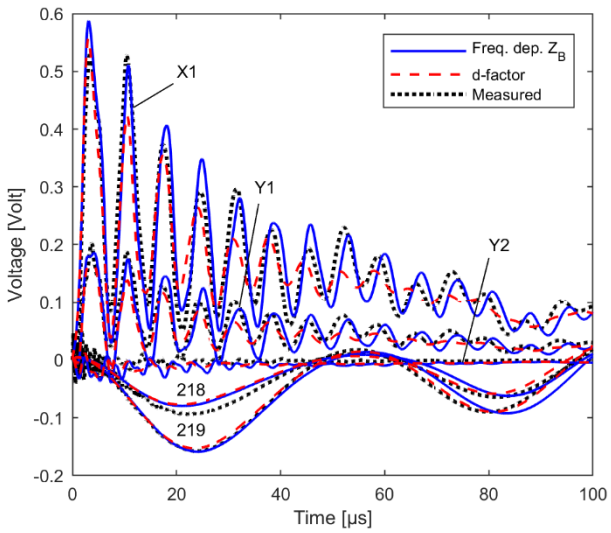

Fig. 14. Simulation result using *d*-factor model. Comparison with proposed model (using phase domain fitting of $\mathbf{Z}_B$) and measurement.

X. Internal Voltage Stresses

The following demonstrates by a simple example the ability of the model to predict the internal voltage stresses that can occur in a transformer when in service.

Fig. 15 shows an example where the tertiary windings of three 1-ph units are connected in delta using 1 mΩ resistors, giving a 3-ph bank. Each 1-ph unit is in the schematic represented by a white box, with labels 1, 2, 3, and 4 representing H1, X1, Y1 and Y2, respectively. The 230 kV primary side is fed via three 1000 mm^2 XLPE SC cables of 484 m length, which are modeled as three uncoupled, frequency-dependent traveling wave models. The cable characteristic impedance and propagation velocity are approximately 31 Ω and 179 m/μs, respectively. The cables are connected to a power system that is represented by a three-phase Thevenin equivalent with a 50 mH short-circuit inductance. The LV terminals are connected to 3 nF capacitors that represent short cables. An ideal ground fault occurs in one phase at the cable feeding end, near voltage maximum (t=10 μs). The ground fault is represented by an ideal switch.

Fig. 16 shows the node-ground voltages in the HV winding connected to the faulted cable (nodes 182-213 in Fig. 4). Before the fault occurs, the voltage is linearly distributed along the winding. The onset of the ground fault at t=10 μs causes a voltage wave to propagate into the cable, which is reflected back-and-forth between the transformer terminal and the fault location. The resulting voltage on the transformer terminal becomes a square-like oscillating voltage. The simulated result is practically the same whether using a rational model for $\mathbf{Z}_B$ obtained by the phase domain or modal domain approach.

Fig. 17 shows every second node-ground voltage in the LV winding (nodes 85-149 in Fig. 4), in the time range 0-100 μs. A Resonance between the cable and the transformer causes the voltage in the LV-winding to increase substantially, compared to the 60 Hz voltage distribution. Such voltage increase can pose a risk to both the transformer and the equipment connected to its LV terminals. Again, the two models (phase domain and modal domain fitting of $\mathbf{Z}_B$) give nearly the same result.

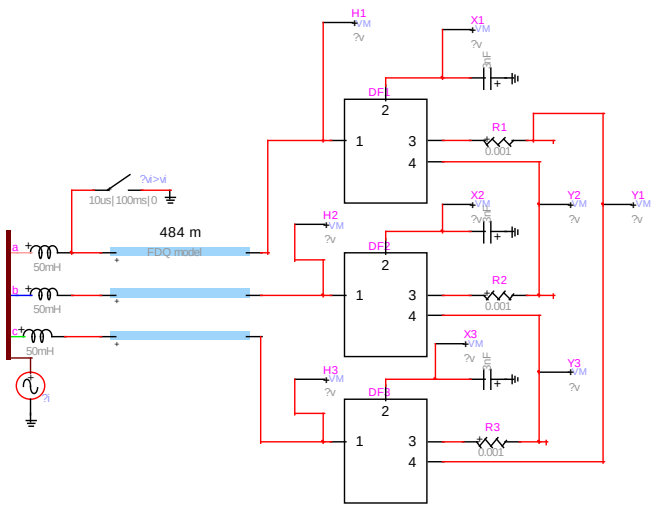

Fig. 15. EMTP simulation model with ground fault applied at t=10 µs at cable feeding end. Labels 1, 2, 3 and 4 represent H1, X1, Y1 and Y2.

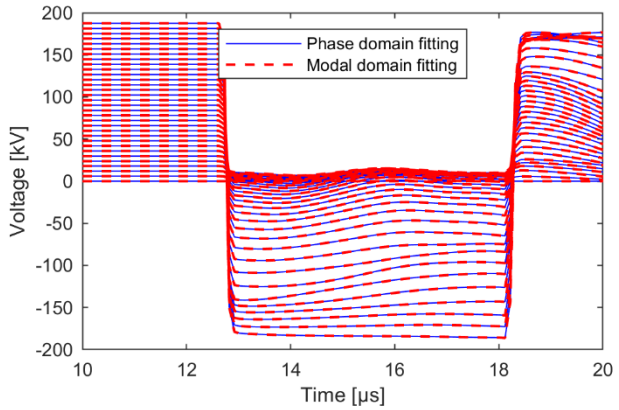

Fig. 16. Ground fault initiation. Voltage in HV winding (nodes 182-213).

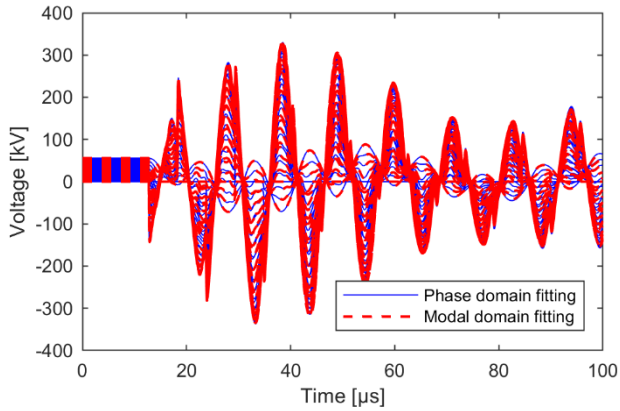

Fig. 17. Ground fault initiation. Voltage in LV winding (nodes 85-149).

XI. Discussion

A. Phase Domain vs. Modal Domain Fitting

For the studied transformer, the two fitting approaches for $\mathbf{Z}_B$ give a very similar result for the transient voltage waveforms produced by the final model, independent of the frequency chosen for diagonalization. Although this result suggests that the frequency dependency of the modal transformation matrix is of little importance, a different conclusion could be reached for other transformers.

The phase domain fitting of $\mathbf{Z}_B$ gives in principle the most accurate model because no simplifications are made, except for the rational fitting itself. With the applied LS weighting schemes, only small passivity violations appeared that were easily removed by RP-NNLS. This may not necessarily be the case for a different transformer. If large passivity violations occur, it may then become a time-consuming task to remove all violations. In that sense, the use of the modal domain fitting method is advantageous because it requires to fit and enforce passivity for a set of independent, scalar problems. This leads to much faster fitting and the passivity enforcement is now much faster and more robust as well.

B. Symmetry Enforcement for Branch Impedance Matrix

It is advantageous to make use of the time domain implementation for the *d*-factor model [7] for EMTP, which yields highly efficient time domain simulations. That implementation requires the diagonalized state-space model (16a), (16b), (16c) to have parameters that are real-valued or complex conjugate. To achieve this property, it is with the phase domain modeling of $\mathbf{Z}_B$ necessary to enforce that the poles and residue matrices are real-valued, and that the residue matrices are symmetrical. This restriction, which was used in this work, leads to a real-valued, unsymmetrical state-matrix in (14a), which has real-valued and complex-conjugate eigenvalues. Similarly, enforcement of real poles is also necessary for modal domain fitting of $\mathbf{Y}_B$. Failing to enforce the real-valued property will cause the final, diagonal model to have parameters that are general complex.

C. Model Validation by NLT

An efficient NLT procedure for validating the EMTP model was presented, based on calculating an alternative, more accurate model for $\mathbf{Z}_B$ (without passivity enforcement), from which new sample values are calculated in the (complex) Laplace domain via nodal analysis. The corresponding time domain samples are calculated by FFT. Such validating samples can in general capture errors in the modeling procedure itself and in the model interfacing with an EMT program.

D. Direct Fitting of Inverse Branch Impedance Matrix

It was also attempted (not shown) to perform phase domain modeling of $\mathbf{Y}_B = \mathbf{Z}_B^{-1}$, thereby avoiding the need for interchanging input and output to recover a model for $\mathbf{Y}_B$ (Section V.D). But that approach was found to give large passivity violations at low frequencies.

E. D-factor Method

The usage of a frequency-dependent $\mathbf{Z}_B$ was in Section IX shown to give a substantially better agreement with a measurement than usage of a frequency-dependent damping factor. The comparison used a damping factor from Fergestad, obtained by measurements on 25 transformers, [11], [31]. It is remarked that a different damping factor was used in the comparison in [12] for the same transformer, which gave a better agreement with the measurement. However, that

damping factor was obtained from the measurement of the transformer, and such measurements are usually not available.

F. Computational Efficiency of Final Model in Time Domain

The time domain simulation is based on a discretization of the state-space model (16a)-(16c) where $\mathbf{A}$ is diagonal [7]. Consider the simulation of all internal node voltages. The CPU time is approximately proportional to the number of elements in $[\mathbf{C}_1^T \quad \mathbf{C}_2^T]^T$, i.e., $N(N+PM) \approx N^2(1+P) \approx N^2 P$. It follows that the CPU time is approximately proportional to the square of the number of nodes N and to the order P of the branch impedance model. Given the small CPU time of the model with $N = 219$ and $P = 6$ in Table VII, it follows that the model will remain efficient also for models with more nodes N, given that the smoothness of $\mathbf{Z}_B$ will allow for use of a low-order P.

For comparison, the number of elements in $\mathbf{C}$ is with the *d*-factor model $N(N+M) \approx 2N^2$. With the given example one could expect about 3.5 times faster calculation with the *d*-factor model, which compares well with the observed ratio of 4.0 (0.53 sec vs. 2.1 sec).

G. Black-Box Variant

If a manufacturer wishes to share a model with a customer, it is possible that he will not allow the calculation of internal voltages. Such restriction is easily achieved when using the proposed model interfacing as one can then simply exclude the matrix $\mathbf{C}_2$ in (16c) from the model, giving a black-box model.

XII. Conclusion

A robust and efficient procedure for white-box transformer modeling and validation has been presented that includes frequency-dependency in the branch impedance matrix $\mathbf{Z}_B$ via rational function approximation.

Two alternative methods are proposed for the rational modeling of $\mathbf{Z}_B$, 1) phase domain modeling of $\mathbf{Z}_B$, and 2) modal domain modeling of $\mathbf{Y}_B = \mathbf{Z}_B^{-1}$. Both methods can extract a model of the branch impedance matrix that is guaranteed passive. The phase domain model is slightly more accurate while the modal domain model is faster to calculate and requires a less sophisticated method for the passivity enforcement. An efficient procedure for accuracy validation of the final (complete) white-box model in the time domain is proposed, based on the Numerical Laplace Transform (NLT).

The final model is compatible with a previously developed model interface for EMTP. Time domain simulation of 5000 time steps for a transformer represented with *N*=219 nodes and a 6th order model of a 213×213 $\mathbf{Z}_B$ required only 0.43 sec for obtaining the four external voltages. The CPU time increased to 2.1 sec if all 219 node voltages were to be simulated.

The combination of high accuracy and EMTP compatibility by an efficient time domain implementation makes the model eminently suited for general network studies, allowing both external and internal overvoltages to be calculated with improved accuracy in a short time. The high computational efficiency is in particular important if the model is to be applied in statistical switching studies, or in Monte Carlo simulation of lightning stroke overvoltages.

The proposed modeling approach requires the availability of frequency domain samples for $\mathbf{Z}_B$, which normally would come from CPU intensive FEM calculations. The method is therefore complementary to the less accurate *d*-factor modeling approach, which requires as input only the capacitance matrix and the high-frequency branch inductance matrix.

XIII. Acknowledgement

The author would like to thank Prof. Enrique Mombello, Universidad Nacional de San Juan, Argentina, for providing the transformer data set used in this work, and Alvaro Portillo, Montevideo, Uruguay, for useful discussions. The members of CIGRE JWG A2/C4.52 are thanked for providing the transformer measurement used in Fig. 14.

XIV. References

[1] R.M. Del Vecchio, B. Poulin, P.T. Feghali, D.M. Shah, and R. Ahuja, *Transformer design principles*, CRC Press, 2010.

[2] W.J. McNutt, T.J. Blalock, R.A. Hinton : "Response of Transformer Windings to System Transient Voltages", *IEEE Trans. Power Apparatus and Systems*,Vol. PAS-93, Issue 2, 1974, pp 457-467.

[3] A. Semlyen, F. De León: "Eddy current add-on frequency dependent representation of winding losses in transformer models used in computing electromagnetic transients", *IEE Proc. Gener. Transm. Distrib*., Vol.141, N°3, May 1994, pp 209-214.

[4] CIGRE Technical Brochure 577A, "Electrical transient interaction between transformers and the power system. Part 1 – Expertise", CIGRE JWG A2/C4.39, April 2014.

[5] CIGRE JWG A2/C4.52, "High-frequency transformer and reactor models for network studies. Part A – White-box models", in press.

[6] B. Gustavsen and A. Portillo, "Interfacing *k*-factor based white-box transformer models with electromagnetic transients programs", *IEEE Trans. Power Delivery*, vol. 29, no. 6, pp. 2534-2542, Dec. 2014.

[7] B. Gustavsen, C. Martin, A. Portillo, "Time domain implementation of damping factor white-box transformer model for inclusion in EMT simulation programs", *IEEE Trans. Power Delivery*, vol. 35, no. 2, pp. 464-472, April 2020.

[8] B. Gustavsen, A. Portillo, "A black-box approach for interfacing white-box transformer models with electromagnetic transients programs", IEEE PES GM 2014, Washington DC, July 27-31, 2014, 5 p.

[9] E. E. Mombello, "New compact white-box transformer model for the calculation of electromagnetic transients," *IEEE Trans. Power Delivery*, vol. 37, no. 4, pp. 2921-2931, Aug. 2022.

[10] CIGRE JWG A2/C4.52, "High-frequency transformer and reactor models for network studies. Part E – Measurements and design data", in press.

[11] P. I. Fergestad and T. Henriksen, "Transient oscillations in multiwinding transformers," *IEEE Trans. Power App. Syst.*, vol. PAS-93, no. 2, pp. 500–509, Mar. 1974.

[12] B. Gustavsen, A. Portillo, "A damping factor-based white-box transformer model for network studies", *IEEE Trans. Power Delivery*, vol. 33, no. 6, pp. 2956-2964, Dec. 2018.

[13] G. A. Diaz, E. E. Mombello, J. P. G and H. K. Høidalen, "Methodology for fast calculation of impedance matrix of power transformers for high frequency transient studies," *IEEE Trans. Power Delivery*, 2022, doi: 10.1109/TPWRD.2022.3209878.

[14] E. E. Mombello, Á. Portillo and G. A. D. Flórez, "New state-space white-box transformer model for the calculation of electromagnetic transients," *IEEE Trans. Power Delivery*, vol. 36, no. 5, pp. 2615-2624, Oct. 2021.

[15] B. Gustavsen, and A. Semlyen, "Rational approximation of frequency domain responses by vector fitting", *IEEE Trans. Power Delivery*, vol. 14, no. 3, pp. 1052-1061, July 1999.

[16] B. Gustavsen, "Passivity enforcement by residue perturbation via constrained non-negative least squares", *IEEE Trans. Power Delivery*, vol. 36, no. 5, pp. 2758-2767, October 2021.

[17] B. Gustavsen, "Passivity assessment and enforcement utilizing eigenpairs information", *Electric Power Systems Research* 194 (2121), 107041.
[18] B. Gustavsen, and A. Semlyen, "Enforcing passivity for admittance matrices approximated by rational functions", *IEEE Trans. Power Systems*, vol. 16, no. 1, pp. 97-104, Feb. 2001.
[19] P. Moreno and A. Ramirez, "Implementation of the Numerical Laplace Transform: A review task force on frequency domain methods for EMT Studies", *IEEE Trans. Power Delivery*, vol. 23, no. 4, pp. 2599-2609, October 2008.
[20] CIGRE JWG A2/C4.52. "High-frequency transformer and reactor models for network studies. Part C – Model interfacing and specifications", in press.
[21] The vector fitting webs site, https://www.sintef.no/projectweb/vectorfitting/
[22] D. Deschrijver, M. Mrozowski, T. Dhaene, and D. De Zutter, "Macromodeling of multiport systems using a fast implementation of the vector fitting method", *IEEE Microwave and Wireless Components Letters*, vol. 18, no. 6, pp. 383-385, June 2008.
[23] V. Brandwajn, "Modification of user's instructions for "MARTI SETUP"", EMTP Newsletter, vol. 3, no. 1, pp. 76-80, August 1982.
[24] S. Grivet-Talocia and B. Gustavsen, *Passive Macromodeling: Theory and Applications*, John Wiley and Sons, 2015.
[25] E.S. Banuelos-Cabral, B. Gustavsen, J.A. Gutierrez-Robles, H.H. Høidalen, J.L. Naredo, "Computational efficiency improvement of the universal line model by use of rational approximations with real poles", *Electric Power Systems Research*, 140 (2116), pp. 424-434.
[26] B. Gustavsen, "Fast passivity enforcement for pole-residue models by perturbation of residue matrix eigenvalues", *IEEE Trans. Power Delivery*, vol. 23, no. 4, pp. 2278-2285, October 2008.
[27] B. Gustavsen, "Computer code for rational approximation of frequency dependent admittance matrices", *IEEE Trans. Power Delivery*, vol. 17, no. 4, pp. 1093-1098, October 2002.
[28] G.H. Golub and C.F. Van Loan, *Matrix Computations*, John Hopkins University Press, Second Ed., 1989. ISBN 0-8018-3772-3.
[29] A. Semlyen and B. Gustavsen, "A half-size singularity test matrix for fast and reliable passivity assessment of rational models", *IEEE Trans. Power Delivery*, vol. 24, no. 1, pp. 345-351, Jan. 2009.
[30] L.M. Wedepohl, "Power system transients: Errors incurred in the numerical inversion of the Laplace transform," in *Proc. 26th Midwest Symp. Circuits Systems*, Aug. 1983, pp. 174–178.
[31] P. Fergestad, "Transient oscillations in transformer windings", PhD Thesis, NTH, Trondhim Norway, 1972. ISBN 82 00 25096 2.
[32] B. Gustavsen, A. Portillo, R. Ronchi, A. Mjelve, "Measurements for validation of manufacturer's white-box transformer models", 4th Int. Colloquium Transformer Research and Asset Management, May 10-12, 2017, Pula, Croatia. Procedia Engineering 202 (2117), pp. 240-250.

BIOGRAPHY

Bjørn Gustavsen (M'94–SM'2003–F'2014) was born in Norway in 1965. He received the M.Sc. degree and the Dr. Ing. degree in Electrical Engineering from the Norwegian Institute of Technology in Trondheim, Norway, in 1989 and 1993, respectively. Since 1994 he has been working at SINTEF Energy Research, currently as Chief Research Scientist. His interests include simulation of electromagnetic transients and modeling of frequency dependent effects. He spent 1996 as a Visiting Researcher at the University of Toronto, Canada, and the summer of 1998 at the Manitoba HVDC Research Centre, Winnipeg, Canada. He was Marie Curie Fellow at the University of Stuttgart, Germany, August 2001–August 2002. He is convenor of CIGRE JWG A2/C4.52.